

Optimal Control of Crystal Size and Shape in Batch Crystallization Using a Bivariate Population Balance Modeling

Marcellus G. F. de Moraes*. Martha A. Grover**. Maurício B. de Souza Jr.*. Paulo L. C. Lage*. Argimiro R. Secchi*

*Chemical Engineering Program - COPPE, Universidade Federal do Rio de Janeiro, Rua Horácio Macedo, 2030, Bloco G, Cidade Universitária, Rio de Janeiro, 21941-914, Brazil (e-mail: marcellus@peq.coppe.ufrj.br, mbsj@eq.ufrj.br, paulo@peq.coppe.ufrj.br, arge@peq.coppe.ufrj.br)

**School of Chemical & Biomolecular Engineering, Georgia Institute of Technology, 311 Ferst Dr. NW, Atlanta, GA, 30332-0100 USA (e-mail: martha.grover@chbe.gatech.edu)

Abstract: An optimal control framework was employed to obtain optimal supersaturation/temperature policies for controlling the crystal mass, size, and shape that meet target product specifications. It uses a bivariate population balance model that includes crystal nucleation, growth, dissolution, and disappearance. The optimal control scheme, solving a dynamic optimization problem, was applied to the batch cooling crystallization of potassium dihydrogen phosphate. The population balance model was evaluated in open-loop experiments, showing good prediction for the mean characteristic lengths and number of particles, both for the supersaturation and undersaturation zones. The deterministic optimal control simulations demonstrated the application of the control action policies to produce crystals of desired mass and average shape for different control targets.

Keywords: crystallization; dynamic optimization; shape control; population balance; optimal control

1. INTRODUCTION

Crystallization is a chemical process prevalent in the industry, being characterized as a solid-liquid separation technique that generates products with a high degree of purity, in a single step, with a low degree of energy demand. Such capacity makes crystallization an attractive technique for the manufacture of many solid materials, especially fine chemicals, and drugs. Due to the complexity of the phenomena involved in crystallization, it is challenging to model and control these processes to achieve the desired product quality and process efficiency.

Population balance models are traditionally used for crystallization processes. Such models are often used in the literature with three main objectives (Lewis et al., 2015): as a predictive model of the size and shape of the particles once a kinetic model has been established, for the proper estimation of the kinetic model parameters from experimental results, and for control and optimization of process conditions in order to obtain a desired size or shape distribution of the crystals, given an already established kinetic model.

The development of adequate control strategies depends on the search for representative models, combined with analytical instrumental technological advancement, which currently arouses growing research interest (Gao et al., 2017; Nagy and Braatz, 2012). Specifically, concerning the control objectives in batch crystallizers, there is a wide variety of

control strategies due to the alternatives of manipulating variables in non-continuous systems to achieve a specific operational or production objective. In a classical review, Rawlings et al. (1993) discussed temperature policies to achieve optimal control of the average crystal size. The use of an open-loop strategy using temperature cycles is employed by Nagy et al. (2011), adopting an optimal temperature policy to eliminate fines, by allowing dissolution cycles.

About model-based control schemes, the use of the MPC (Model Predictive Control) becomes viable and increasingly attractive if the model's output variables can be measured and monitored, such as, for example, the concentration of the solute and the crystal size distribution (Damour et al., 2010; Kalbasenka et al., 2012). The dynamic programming approach is also a model-based scheme to establish the control policy, but control input policies can be calculated offline a priori and stored. In this way, it has the advantage of making it possible to close the loop more simply in practice. The dynamic programming in crystallization control is reported using empirical models, such as Markov State Model based on experimental measurements (Griffin et al., 2016; Grover et al., 2020).

In addition to the concern with the particle size, modeling for the shape (crystal habit) may be necessary and of progressive use in the development of predictive modeling and control of crystallization processes. However, controlling the particle shape presents an additional difficulty, both from the point of view of the model design and the measurement of important

variables during the process. The number of control studies related to crystal shape is yet limited (Bötschi et al., 2018). For these cases, the use of multidimensional PBM, in turn, presents greater complexity, mainly due to the difficulty of experimental measurements of the size of the crystals in multiple directions combined with possible computational difficulties for their solution.

The use of temperature cycling experiments (using growth-dissolution cycles) as a strategy to modify the crystal shape was studied in the past. Jiang et al. (2014) estimate both size-dependent growth and dissolution kinetics parameters in a 2D-PBM solved using the method of characteristics. In that study, the authors predicted the crystal shape for the monosodium glutamate. Eisenschmidt et al. (2016) developed an optimal control scheme based on the temperature cycling strategy, showing experimentally the efficiency of controlling the crystal shape through two dimensions of crystals of potassium dihydrogen phosphate (KDP). The size-independent growth and dissolution kinetics for KDP were previously estimated from experiments at constant supersaturation and undersaturation levels (Eisenschmidt et al., 2015). In that study, the authors defined a region in state space to track only the seed crystal evolution, thus disregarding nucleation and disappearance phenomena.

Regarding crystal shape control, a simulation control study that evaluated the effects of optimal control policies and spatial variations on crystal shape was performed (Ma et al., 2002). A 2D-PBM considering only growth phenomenon for the L-glutamic acid was developed and applied experimentally in closed-loop feedback control for experiments with different control targets (Yang et al., 2012). Using this same approach and still taking into account only the phenomenon of crystal growth, optimal temperature control, and optimal supersaturation control were compared in terms of performance in achieving the shape control targets in a real crystallizer for the L-glutamic acid (Ma et al., 2012).

A simulation study applying a less complex size and shape control approach that does not need kinetic models for a crystallization process considering only growth proves efficient (Bötschi et al., 2018). This model-free approach, called path following control (PFC) proved attractive compared with more complex schemes such as NMPC (Nonlinear Model Predictive Control) that require the availability of growth rates. The experimental validation of PFC as a suitable feedback control scheme for shape was obtained for the β L-glutamic acid crystallization (Rajagopalan et al., 2019).

For crystal shape control in a continuous process, an NMPC was developed by Kwon et al. (2014a) to control the shape of lysozyme crystals using a mixed suspension mixed product removal (MSMPR) reactor with a fine-particle trap. Good results were obtained for the regulation of the average crystal aspect ratio operating in a growth cycle. The authors employed an 1D moment model for the crystal volume distribution. A feed-forward control was designed by Kwon et al. (2014b) for the lysozyme crystals using a plug flow

configuration, producing crystals with desired size and shape under feed flow disturbance rejection.

In this study, a bivariate population balance model (2D-PBM) was developed for KDP. The 2D-PBM was developed for supersaturated and undersaturated conditions, making it possible to use temperature cycling to achieve the desired product specification. The good agreement of the model prediction with experimental results makes the 2D-PBM approach attractive in optimal control strategy to reach targets of mass, size, and shape of KDP crystals.

2. METHODS

2.1 Model development

For modeling the morphology of KDP crystals, two characteristic dimensions called L_1 and L_2 were used as internal coordinates of the population balance equation (PBE). KDP crystals have a crystalline habit, as shown in Fig. 1, and the choice of the two characteristic lengths was also used by Yang et al. (2006), Ma et al. (2002) and Gunawan et al. (2002).

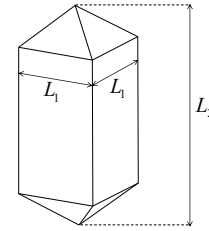


Fig. 1: KDP crystal and the characteristics lengths.

Taking into account these two internal variables in the state space, a bivariate number density distribution $n(L_1, L_2, t)$ is established, in [$\# / (\mu\text{m}^2 \cdot \text{cm}^3 \text{ of solvent})$].

In this work, the supersaturation S was considered as the driving force and input variable:

$$S = c / c^* \quad (1)$$

where c is the solute concentration and c^* is solute equilibrium concentration, in [$\text{g of solute} / \text{cm}^3 \text{ of solvent}$]. The variation of the solvent density with temperature was neglected.

First, for supersaturated conditions ($S > 1$), the phenomena considered were the crystal growth and nucleation, and the PBE applied to the batch crystallizer yields:

$$\frac{\partial n}{\partial t} + \frac{\partial(G_1 n)}{\partial L_1} + \frac{\partial(G_2 n)}{\partial L_2} = B \delta(L_1) \delta(L_2) \quad (S \geq 1) \quad (2)$$

where G_1 (3) and G_2 (4) are the crystal growth rates in [$\mu\text{m} / \text{min}$], B denotes the nucleation rate in [$\# / (\text{min} \cdot \text{cm}^3 \text{ of solvent})$] (5), and $\delta(\cdot)$ is the Dirac delta function.

$$G_1 = k_{g,1} \exp\left(-\frac{E_{a_{g,1}}}{RT}\right) S^{\alpha_{g,1}} \quad (3)$$

$$G_2 = k_{g,2} \exp\left(-\frac{E_{a_{g,2}}}{RT}\right) S^{\alpha_{g,2}} \quad (4)$$

$$B = k_b \exp\left(-\frac{E_{a_b}}{RT}\right) S^{\alpha_b} M_T^\beta \quad (5)$$

where $k_{g,1}$, $k_{g,2}$ and k_b are pre-exponential constants; $E_{a_{g,1}}$, $E_{a_{g,2}}$ and E_{a_b} are activation energies; M_T is the mass of crystals per solvent volume; $\alpha_{g,1}$, $\alpha_{g,2}$, α_b and β are exponent parameters; R is the universal gas constant; and T is the suspension temperature.

For undersaturated conditions ($S < 1$), the PBE yields:

$$\frac{\partial n}{\partial t} + \frac{\partial(D_1 n)}{\partial L_1} + \frac{\partial(D_2 n)}{\partial L_2} = 0 \quad (S < 1) \quad (6)$$

where D_1 and D_2 are the crystal dissolution rates in [$\mu\text{m}/\text{min}$], $D_1, D_2 < 0$ (7,8).

$$D_1 = -k_{d,1} \exp\left(-\frac{E_{a_{d,1}}}{RT}\right) S^{\alpha_{d,1}} \quad (7)$$

$$D_2 = -k_{d,2} \exp\left(-\frac{E_{a_{d,2}}}{RT}\right) S^{\alpha_{d,2}} \quad (8)$$

where $k_{d,1}$ and $k_{d,2}$ are pre-exponential constants; $E_{a_{d,1}}$, $E_{a_{d,2}}$ are activation energies; $\alpha_{d,1}$ and $\alpha_{d,2}$ are exponent parameters.

In this case of $S < 1$, the solute concentration is lower than the solubility, and crystals can dissolve continuously and in the extremal case, some fines may disappear.

2.2 Cross-moment equations and numerical approach

Moments of the crystal size distribution were decided to be used as state variables (and also measured variables by image analysis) for the purpose of the crystal size and shape control in this work. Using the method of moments, the cross-moments $\mu_{i,j}$ defined in the space of two dimensions are given by:

$$\mu_{i,j} = \int_0^\infty \int_0^\infty L_1^i L_2^j n(L_1, L_2, t) dL_2 dL_1 \quad (9)$$

When applying the cross-moment integral transform operator to (2) and (6), the following cross-moment set of ODEs is obtained.

For $i, j \geq 1$:

$$\begin{aligned} \frac{d\mu_{i,j}}{dt} &= i G_1 \mu_{i-1,j} + j G_2 \mu_{i,j-1}, \quad i, j \geq 1 \quad (S \geq 1) \\ \frac{d\mu_{i,j}}{dt} &= i D_1 \mu_{i-1,j} + j D_2 \mu_{i,j-1}, \quad i, j \geq 1 \quad (S < 1) \end{aligned} \quad (10)$$

The integral transformation for the moment equations of $\mu_{i,0}$ yields:

$$\begin{aligned} \frac{d\mu_{i,0}}{dt} &= i G_1 \mu_{i-1,0} \quad (S \geq 1) \\ \frac{d\mu_{i,0}}{dt} &= i D_1 \mu_{i-1,0} + D_2 \int_0^\infty L_1^i n(L_1, 0, t) dL_1 \quad (S < 1) \end{aligned} \quad (11)$$

In the same way, for $\mu_{0,j}$:

$$\begin{aligned} \frac{d\mu_{0,j}}{dt} &= j G_2 \mu_{0,j-1} \quad (S \geq 1) \\ \frac{d\mu_{0,j}}{dt} &= j D_2 \mu_{0,j-1} + D_1 \int_0^\infty L_2^j n(0, L_2, t) dL_2 \quad (S < 1) \end{aligned} \quad (12)$$

For the zeroth order cross moment $\mu_{0,0}$:

$$\begin{aligned} \frac{d\mu_{0,0}}{dt} &= B \quad (S \geq 1) \\ \frac{d\mu_{0,0}}{dt} &= D_2 \int_0^\infty n(L_1, 0, t) dL_1 + D_1 \int_0^\infty n(0, L_2, t) dL_2 \quad (S < 1) \end{aligned} \quad (13)$$

For undersaturated conditions ($S < 1$), it was experimentally observed that $L_2 > L_1$ at any time. Therefore, the outgoing particle flux at the $L_2 = 0$ boundary, that is $D_2 n(L_1, 0, t)$, is zero, and the characteristic curves leave the domain only at the $L_1 = 0$ plane. Consequently, the terms

$$D_2 \int_0^\infty L_1^i n(L_1, 0, t) dL_1 \quad \text{in (11) and } D_2 \int_0^\infty n(L_1, 0, t) dL_1 \quad \text{in (13)}$$

are null. Additionally, under the assumption that L_2 is close to zero when $L_1 = 0$, the high-order ($j > 0$) moment fluxes

$$D_1 \int_0^\infty L_2^j n(0, L_2, t) dL_2 \quad \text{in (12) can be neglected.}$$

However, the evaluation of the flux $D_1 \int_0^\infty n(0, L_2, t) dL_2$ is needed in (13) to close the model. Defining the marginal density distribution $n_{L_1}(L_1, t)$ as:

$$n_{L_1}(L_1, t) = \int_0^\infty n(L_1, L_2, t) dL_2, \quad (14)$$

this particle flux is given by $D_1 n_{L_1}(0, t)$. The equation for n_{L_1} is obtained by integrating (6) in the whole L_2 domain, being given by:

$$\frac{\partial n_{L_1}}{\partial t} + D_1 \frac{\partial n_{L_1}}{\partial L_1} = 0 \quad (S < 1) \quad (15)$$

where the particle flux at $L_2 = 0$ was again not considered due to the experimental evidence that $L_2 > L_1, \forall t$. The numerical calculation of (15) is less laborious and have a lower computational cost when compared to the calculations of n using (6). For (15), the high-resolution finite volume method ("HR- $\kappa = -1$ scheme") by Qamar et al. (2006) was employed.

In this way, having the marginal density distribution at the boundary $L_1 = 0$ by solving (15), the number of particles that leave the domain per solvent volume, N_d [# / cm³], can be accounted during a sampling time Δt by the following integral:

$$N_d(t) = - \int_{t-\Delta t}^t D_1 n_{L_1}(0, \xi) d\xi \quad (16)$$

Thus, (13) for $S < 1$ can be explicitly integrated in one time step to give:

$$\mu_{0,0}(t) = \mu_{0,0}(t - \Delta t) - N_d \quad (17)$$

In order to relate third order cross-moments with the mass of crystals and solute concentration, the volume of a single KDP crystal can be expressed by (Borchert, 2012; Ma et al., 2002):

$$V_c(t, L_1, L_2) = L_2 L_1^2 - \frac{2}{3} L_1^3 \quad (18)$$

In this way, the mass of crystal per solvent volume M_T can be expressed by:

$$M_T = \rho_c \left(\mu_{2,1} - \frac{2}{3} \mu_{3,0} \right) \quad (19)$$

The crystal mass balance can be defined, in the same manner, by:

$$\frac{dm_c(t, L_1, L_2)}{dt} = \rho_c \frac{dV_c(t, L_1, L_2)}{dt} \quad (20)$$

Using (18) and the definition of the growth/dissolution rates:

$$\begin{aligned} \frac{dm_c}{dt} &= \rho_c \left[(2L_1 L_2 - L_1^2) G_1 + L_1^2 G_2 \right], \quad S \geq 1 \\ \frac{dm_c}{dt} &= \rho_c \left[(2L_1 L_2 - L_1^2) D_1 + L_1^2 D_2 \right], \quad S < 1 \end{aligned} \quad (21)$$

By a mass balance and integrating (21) in the whole internal variable domain, the solute concentration equation can be represented by:

$$\begin{aligned} \frac{dc}{dt} &= -\rho_c (2G_1 \mu_{1,1} - G_1 \mu_{2,0} + G_2 \mu_{2,0}), \quad S \geq 1 \\ \frac{dc}{dt} &= -\rho_c (2D_1 \mu_{1,1} - D_1 \mu_{2,0} + D_2 \mu_{2,0}), \quad S < 1 \end{aligned} \quad (22)$$

By switching the model for each zone, the developed approach can describe the system behavior as the temperature is increasing, causing dissolution and disappearance of KDP crystals, and decreasing, causing crystal growth and nucleation.

Based on the structure of the models presented in this section, the kinetic parameters for nucleation, growth, and dissolution were estimated for KDP for a given set of experiments. Details of the adopted approach are described in Moraes et al. (2019). Numerical integration of the model during the parameter estimation process was done by the integrator code DASSLC v3.9 (Secchi, 2014). Section 3.1 presents the results for the model prediction compared to experimental results.

2.3 Experimental Setup

Crystallization and dissolution experiments for KDP (Synth, > 99%) in distilled water were performed in a 1-liter jacketed glass vessel (Syrris[®]) with a two-blade stirrer (Orb[®]) operating at a rate of 400 rpm. A peristaltic pump (MasterFlex L/S) was coupled to the vessel to provide adequate sampling and conduction of the suspension through the image analyzer equipment (QICPIC-LIXELL Sympatec[®]) at a flow rate of 140 cm³/min. This external sampling loop was made online during the experiments. The image analyzer continuously obtained videos of the sample suspension at a frequency of 100 frames per second. At each 1 minute (sampling time), the data was acquired. The images of all crystals captured by the images were used to estimate the state of size and shape. The WINDOX Sympatec[®] software allows real-time monitoring of the solid phase by acquiring variables of size and shape of the crystals (such as the cross-moments).

The temperature measurements were done using a thermocouple in contact with the solution. The thermoregulator (thermostatic bath, Huber[®] Petite Fleur) was connected to the vessel's cooling jacket for temperature control. For the liquid phase (solution), the solute concentration was determined by a conductivity sensor (Gehaka[®] CG2000) in situ. The conductivity (κ) was related to the solute concentration and temperature by a calibration equation:

$$\kappa(c, T) = \alpha_{1,0} T + \alpha_{0,1} c + \alpha_{1,1} T c + \alpha_{0,0} \quad (23)$$

where $\alpha_{1,0}$, $\alpha_{0,1}$, $\alpha_{1,1}$ and $\alpha_{0,0}$ were parameters estimated.

The KDP equilibrium concentration c^* in the following polynomial form, empirically described by Eisenschmidt et al. (2006), was used in this work:

$$c^*(T) = AT^2 + BT + C \quad (24)$$

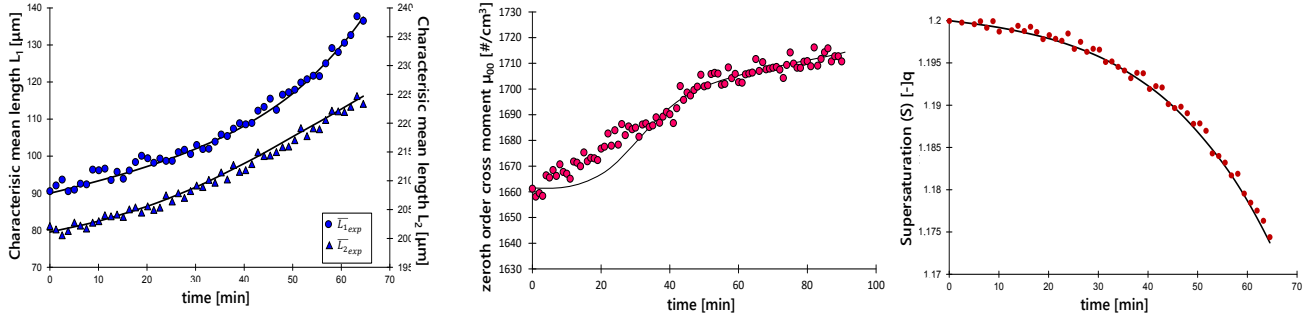


Fig. 3: Precited and experimental values for supersaturation zone experiment: characteristic mean lengths (left), zeroth order cross-moment (middle) and supersaturation (right). Black lines represent the values predicted by the model.

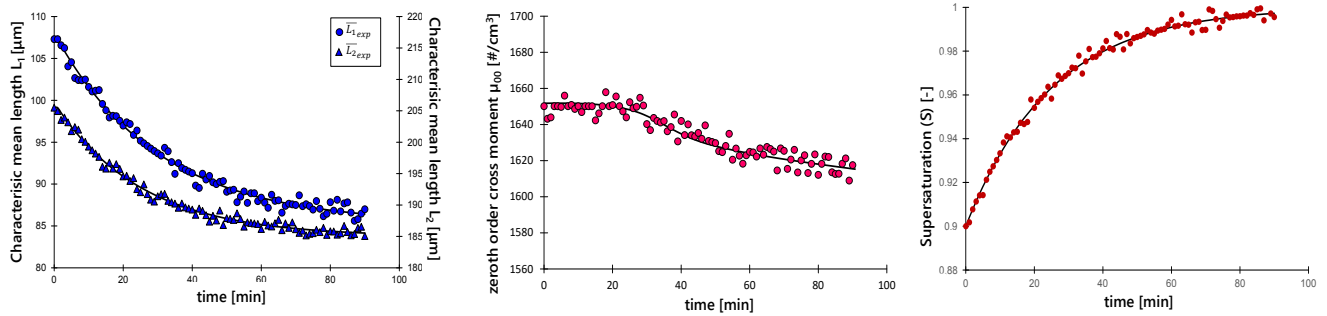


Fig. 4: Precited and experimental values for undersaturation zone experiment: characteristic mean lengths (left), zeroth order cross-moment (middle) and supersaturation (right). Black lines represent the values predicted by the model.

3.2 Simulation Results for Optimal Control

Table 1 shows the run targets and batch times for the 3 deterministic runs performed.

The choice of the spatial orientation using the three variables in (23) allows better visualization of the crystallization trajectory. Using this plot, in addition to checking the yield (mass) of the process, it is possible to follow both the average characteristic lengths L_1 and L_2 (indicating the crystal size).

Table 1: Deterministic runs evaluated

	target \mathbf{x}^\oplus [g, μm , μm]	Batch time [min]
Run 1	[6, 200, 400]	90
Run 2	[8, 60, 200]	90
Run 3	[10, 100, 150]	90

In this way, it is possible to monitor the relative position of L_1 and L_2 along the batch, which indicates the change in the crystal shape by altering the slope of the trajectory, analyzing the $L_1 \times L_2$ plane. It is illustrated by the simulation results for the three runs in Fig. 5.

It is possible to observe different behavior of the trajectory depending on the required final target due to the implemented inputs. For Run 1, it only operates in supersaturation,

obtaining a more straight-forward trajectory, indicating both increased yield and growth of the crystals until they reached

the desired size and shape. For Run 2 and Run 3, the trajectory is perceived in areas of supersaturation and undersaturation.

The temperature policies were obtained from the supersaturation optimal policies combining them with the calibration and equilibrium equations. Furthermore, the simulated control could eliminate the error in the final crystal specification (distance from the target is near zero).

When verifying the crystal shape, Fig. 6 shows that for Run 1, the crystal aspect ratio does not vary significantly over time, indicating that the crystal growth in both directions follows a similar rate while there is an increase in mass until the target is reached. For Run 2 and Run 3, the most pronounced variation in the trajectory inclination (i.e. aspect ratio) is noticeable when changes are made between the regions of $S > 1$ and $S < 1$.

4. CONCLUSIONS

The theoretical model based on a 2D-PBM that incorporates nucleation and growth (in supersaturation zones) and dissolution and disappearance (in undersaturation zones) was obtained for KDP. It showed good predictions for open-loop batch crystallization experiments. The presented optimal control strategy application is experimentally suitable for closed-loop control, calculating the temperature setpoints based on the obtained optimal supersaturation policies. It is expected that this approach will be applied to different compounds and measuring techniques, to investigate not only the mass and size, but also the crystal shape.

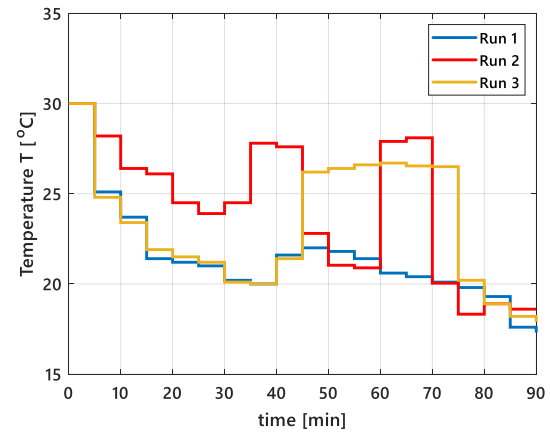
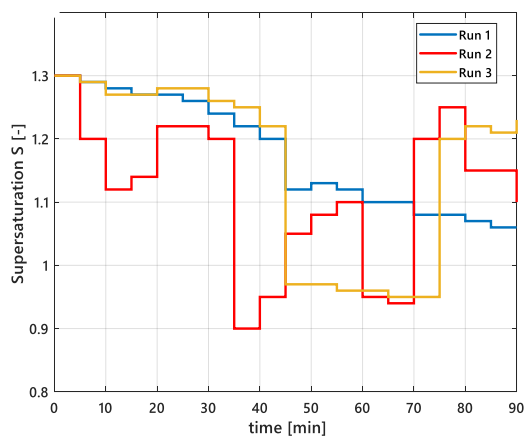
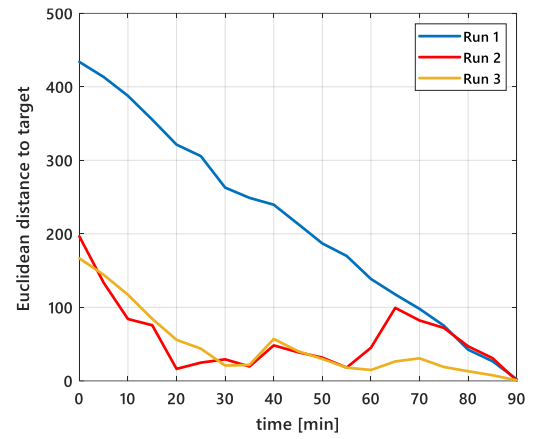
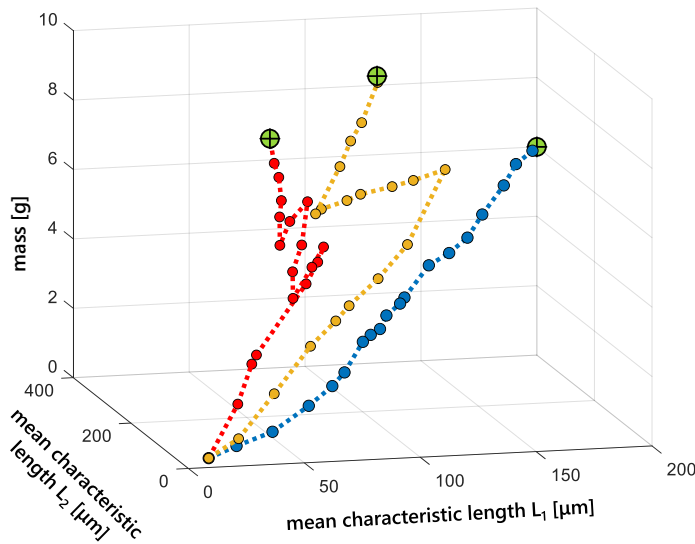


Fig. 5: Simulation results for optimal control for KDP. Above: state trajectories (left); Euclidean distance to target (right). Below: supersaturation optimal control actions (left); temperature policies calculated by supersaturation policies (right).

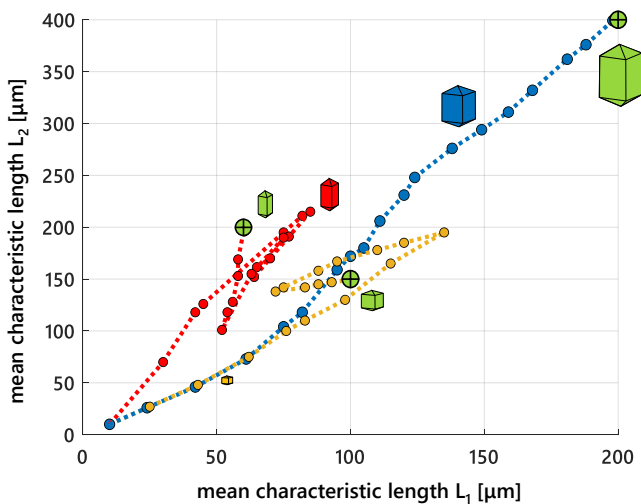


Fig 6: $L_1 \times L_2$ plot. Changes in trajectory slope indicate that aspect ratio changes. Targets are in green. Some scale representations of KDP crystals at different positions in space are shown

ACKNOWLEDGMENT

“This study was financed in part by the Coordenação de Aperfeiçoamento de Pessoal de Nível Superior – Brasil (CAPES) – Finance Code 001”

REFERENCES

- Borchert, C. (2012). *Topics in Crystal Shape Dynamics*. Otto-von-Guericke University, Alemanha: Magdeburg.
- Bötschi, S., Rajagopalan, A. K., Morari, M., Mazzotti, M. (2018). Feedback Control for the Size and Shape Evolution of Needle-like Crystals in Suspension. I. Concepts and Simulation Studies. *Crystal Growth & Design*, v.18, pp. 4470-4483.
- Briesen, H. (2006). Simulation of crystal size and shape by means of a reduced two-dimensional population balance model. *Chemical Engineering Science*, v. 61, n. 1, pp. 104–112.

- Damour, Cédric; Benni, Michel; Boillereaux, Lionel; Grondin-Perez, Brigitte; Chabriat, Jean-Pierre. (2016). NMPC of an industrial crystallization process using model-based observers, *Journal of Industrial and Engineering Chemistry*, v. 16, p. 708-716, 2010.1372.
- Eisenschmidt, H., Voigt, A., Sundmacher, K. (2015). Face-Specific Growth and Dissolution Kinetics of Potassium Dihydrogen Phosphate Crystals from Batch Crystallization Experiments. *Crystal Growth & Design*, v. 15, pp. 219-227.
- Eisenschmidt, H., Bajcinca, N., Sundmacher, K. (2016). Optimal Control of Crystal Shapes in Batch Crystallization Experiments by Growth-Dissolution Cycles. *Crystal Growth & Design*, v. 16, pp. 3297-3306.
- Gao, J., Rohani, G., Gong, J., Wang, J. (2017). Recent Developments in the Crystallization Process: Toward the Pharmaceutical Industry, *Engineering*, v.3, p.343-353.
- Griffin, D. J., Grover, M. A., Kawajiri, Y., Rousseau, R. W. (2016). Data-driven modeling and dynamic programming applied to batch cooling crystallization. *Industrial and Engineering Chemistry Research*, vol. 55, no. 5, pp. 1361.
- Grover, M. A., Griffin, D. J., Tang, X., Kim, Y., Rousseau, R. (2020). Optimal feedback control of batch self-assembly processes using dynamic programming. *Journal of Process Control*, v. 88, p. 32-42.
- Jiang, M., Zhu, X., Molaro, M. C., Rasche, M. L., Zhang, H., Chadwick, K., Raimondo, D. M., Kim, K. K., Zhou, L., Zhu, Z., Wong, M. H., O'Grady, D., Hebrault, D., Tedesco, J., Braatz, R. D. Modification of crystal shape through deep temperature cycling. *Industrial Engineering & Chemistry Research*. 2014, v. 53, p. 5325-5336.
- Kalbasenka, Alex N.; Huesman, Adrie E. M.; Kramer, Herman J. M. (2012). Model Predictive Control. *Industrial Crystallization Process Monitoring and Control*. Wiley-VCH.
- Kwon, JSI., M. Nayhouse, P. D. Christofides and G. Orkoulas, "Modeling and Control of Crystal Shape in Continuous Protein Crystallization," *Chemical Engineering Science*, v.107, p.47-57, 2014a.
- Kwon, JSI., M. Nayhouse, G. Orkoulas and P. D. Christofides, Crystal Shape and Size Control Using a Plug Flow Crystallization Configuration, *Chemical Engineering Science*, v. 119, p. 30-39, 2014b.
- Lewis, A.; Seckler, M.; Kramer, H.; Van Rosmalen, G. (2015). *Industrial Crystallization: Fundamentals and Application*, 1. ed. Cambridge University Press.
- Ma, C. Y., Wang, X. Z. (2012) Closed-loop control of crystal shape in cooling crystallization of l-glutamic acid. *Journal of Process Control*, v. 22, pp. 72-81.
- Ma, D. L.; Tafti, D. K.; Braatz, R. D. (2002). Optimal control and simulation of multidimensional crystallization processes. *Computers & Chemical Engineering*, v. 26, pp. 1103-1116.
- Moraes, M. G. F., Secchi, A. R., Barreto Jr., A. G., Souza Jr., M B. (2019). Measurement and modeling of crystal size and shape distributions of potassium sulfate through dynamic image analysis in batch cooling crystallization, In: *PSE-BR 2019*, Rio de Janeiro, Brazil.
- Nagy, Z. K., Braatz, R. D. (2012). Advances and New Directions in Crystallization Control, *Annual Review of Chemical and Biomolecular Engineering*, v. 3, pp. 55-75
- Nagy, Z. K.; Aamir, E.; Rielly, C. D. (2011). Internal Fines Removal Using Population Balance Model Based Control of Crystal Size Distribution under Dissolution, Growth and Nucleation Mechanisms. *Crystal & Growth Design*, v. 11, pp. 2205-2219.
- Oullion, M.; Puel, F.; Févotte, G.; Righini, S.; Carvin, P. (2007). Industrial batch crystallization of a plate-like organic product. In situ monitoring and 2D-CSD modelling. Part 1: Experimental study. *Chemical Engineering Science*, v. 62, n. 3, pp. 820-832.
- Qamar, S.; Elsner, M. P.; Angelov, I. A.; Warnecke, G.; Seidel-Morgenstern, A. (2006). A comparative study of high resolution schemes for solving population balances in crystallization. *Computers & Chemical Engineering*, 30, 1119-1131.
- Rajagopalan, A. K., Bötschi, S., Morari, M., Mazzotti, M. (2018). Feedback Control for the Size and Shape Evolution of Needle-like Crystals in Suspension. II. Cooling Crystallization Experiments. *Crystal Growth & Design*, v.18, pp. 6185-6186.
- Rawlings, J. B., Miller, S. M., and Witkowski, W. R. (1993). Model identification and control of solution crystallization processes: a review. *Industrial & Engineering Chemistry Research*, v. 32, pp. 1275-1296.
- Secchi, A. R. (2014). *DASSLC User's Manual Version 3.9*. Universidade Federal do Rio Grande do Sul, DEQUI, Porto Alegre, RS, Brazil.
- Wang, X. Z.; Roberts, K. J.; Ma, C. (2008). Crystal growth measurement using 2D and 3D imaging and the perspectives for shape control. *Chemical Engineering Science*, v. 63, n. 5, pp 1173-1184.
- Yang, Y., Ma, C. Y., Wang, X. Z. (2012) Optimisation and Closed-loop Control of Crystal Shape Distribution in Seeded Cooling Crystallisation of L-Glutamic Acid. In: *8th IFAC Symposium on Advanced Control of Chemical Processes*, Singapore, July 10-13, 2012, pp. 216-221.